JACS
JOURNAL OF THE AMERICAN CHEMICAL SOCIETY

ARTICLE

pubs.acs.org/JACS

Fragment Growing Induces Conformational Changes in Acetylcholine-Binding Protein: A Structural and Thermodynamic Analysis

Ewald Edink,[†,#] Prakash Rucktooa,[‡,#] Kim Retra,[†] Atilla Akdemir,[†] Tariq Nahar,[§] Obbe Zuiderveld,[†] René van Elk,[§] Elwin Janssen,[⊥] Pim van Nierop,[§] Jacqueline van Muijlwijk-Koezen,[†] August B. Smit,[§] Titia K. Sixma,[‡] Rob Leurs,[†] and Iwan J. P. de Esch*[,†]

[†]Leiden/Amsterdam Center of Drug Research (LACDR), Division of Medicinal Chemistry, Faculty of Sciences, VU University Amsterdam, The Netherlands

[‡]Divison of Biochemistry, Netherlands Cancer Institute, The Netherlands

[§]Department of Molecular and Cellular Neurobiology, Center for Neurogenomics & Cognitive Research, VU University Amsterdam, The Netherlands

[⊥]Department of Chemistry and Pharmaceutical Sciences, VU University Amsterdam, The Netherlands

Supporting Information

ABSTRACT: Optimization of fragment hits toward high-affinity lead compounds is a crucial aspect of fragment-based drug discovery (FBDD). In the current study, we have successfully optimized a fragment by growing into a ligand-inducible subpocket of the binding site of acetylcholine-binding protein (AChBP). This protein is a soluble homologue of the ligand binding domain (LBD) of Cys-loop receptors. The fragment optimization was monitored with X-ray structures of ligand complexes and systematic thermodynamic analyses using surface plasmon resonance (SPR) biosensor analysis and isothermal titration calorimetry (ITC). Using site-directed mutagenesis and AChBP from different species, we find that specific changes in thermodynamic binding profiles, are indicative of interactions with the ligand-inducible subpocket of AChBP. This study illustrates that thermodynamic analysis provides valuable information on ligand binding modes and is complementary to affinity data when guiding rational structure- and fragment-based discovery approaches.

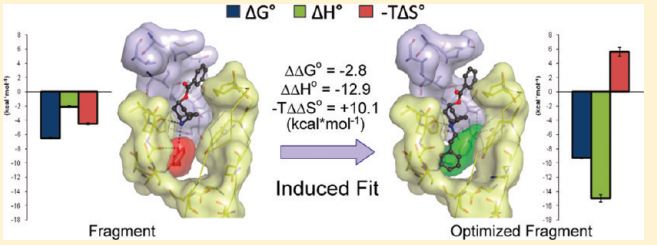

INTRODUCTION

In the past decade, fragment-based drug discovery (FBDD) has become a well-established method in the field of drug discovery.[1−3] Compared to traditional high-throughput screening (HTS), FBDD is based on screening of smaller libraries of compounds (typically containing 1000−5000 fragments) with lower molecular weights (i.e., smaller than 300 Da).[4] Fragment-based screening results in a better coverage of chemical space and usually higher hit rates than HTS.[3,5] Identified fragment hits are either optimized by linking or growing. In fragment linking, two simultaneously binding fragments are connected via a chemical linker. Unfortunately, the expected increase in affinity is often compromised by perturbation of the binding modes of the separate fragments or strain in the linker used to connect the fragments.[6,7] The preferred hit-optimization strategy in FBDD has become fragment growing.[1,8] In iterative cycles, additional features are added to the hit fragment, leading to more-potent compounds. Structural biology has been shown to be crucial to guide the optimization of fragment hits toward novel and potent drugs.[1,3,9−11] In the current study, we employ FBDD approaches to develop new ligands that bind to acetylcholine-binding protein (AChBP). This water-soluble pentameric protein is widely recognized as a structural homologue of the ligand binding domain (LBD) of Cys-loop receptors.[12,13] Currently, AChBPs from different species such as *Lymnaea stagnalis* (Ls-AChBP),[14−16] *Aplysia californica* (Ac-AChBP),[17,18] and *Bulinus truncatus* (Bt-AChBP)[19] have been identified and crystallized, providing high-resolution structural models of the extracellular domains of the pentameric ligand-gated ion channels (LGICs) of the Cys-loop family, such as nicotinic acetylcholine receptors (nAChRs), GABA$_A$-, serotonin 5-HT$_3$-, and glycine receptors.[13]

In a recent study, tropine derivatives were identified as AChBP ligands using an in silico screening protocol.[18] A structural analogue, the benzoate substituted nortropine fragment **1**, exhibits good ligand efficiency (LE)[20] of 0.43 kcal·mol^{-1} per heavy atom for Ac-AChBP and is therefore considered to be a good starting point for further optimization (Figure 1). In the current study, a

Received: November 24, 2010
Published: February 15, 2011

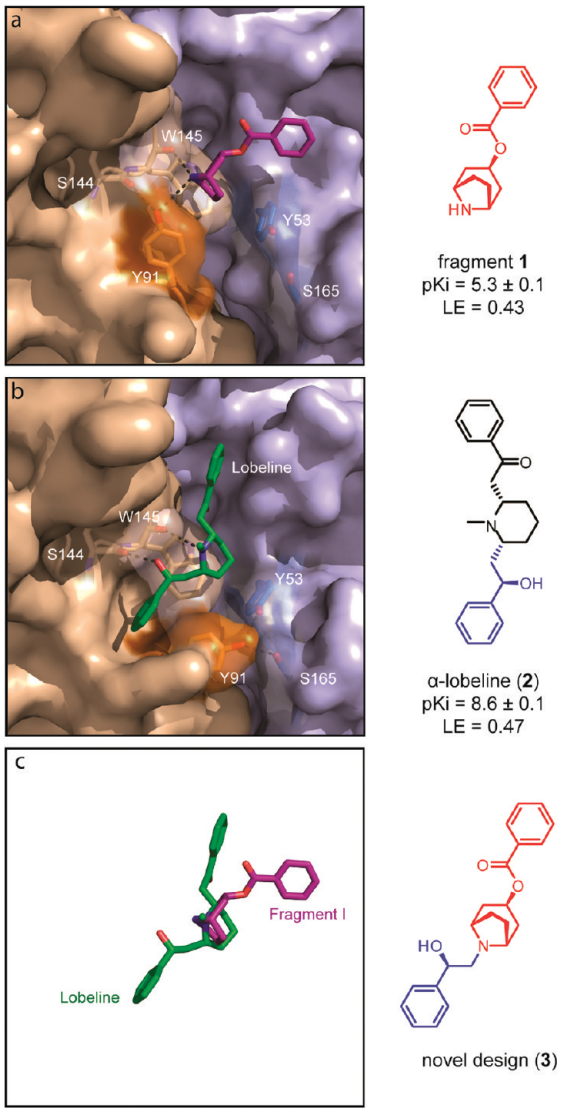

Figure 1. Fragment optimization strategy. Surface representations of the crystal structures of fragment **1**-bound Ac-AChBP (**a**) and of lobeline-bound Ac-AChBP (PDB 2BYS)[16] (**b**). (**a**) In the fragment **1**-Ac-AChBP complex, Tyr91 (orange) is stabilized in the *g*- conformation through a hydrogen bond with Ser144, rendering the lobeline pocket inaccessible. (**b**) However, Tyr91 adopts a *t* conformation in the lobeline−Ac-AChBP complex interacting with Tyr53 and Ser165 through hydrogen bonds, thus leading to the opening of the lobeline pocket. (**c**) The superposition of the fragment **1** and lobeline (**2**) molecules indicates that the fragment may be grown into the lobeline pocket by decorating the tropine nitrogen with the α-hydroxyphenetyl moiety of lobeline generating compound (**3**).

cocrystal complex of fragment **1** and Ac-AChBP was generated, thereby enabling structure-based optimization. Comparison with previously obtained cocrystal complexes reveals conformational changes of the target protein upon ligand binding, mainly with respect to loop C, which closes the binding site upon agonist binding.[15,17−19,21] A unique conformational change is observed for AChBP while binding to lobeline, leading to the opening of a subpocket that enables the binding of the α-hydroxyphenetyl moiety of the ligand.[17] More specifically, the subpocket, which we will refer to as the lobeline pocket, becomes accessible after a change in the rotameric state of Tyr91 (*g*- to *t* conformation,[22] hereafter referred to as the tyrosine-flip). Considering the partially overlapping binding modes of hit fragment **1** and lobeline (**2**), we designed a fragment growing optimization study to induce the tyrosine-flip and grow the fragment into the lobeline pocket (Figure 1). The ligand-induced opening of binding site subpockets represents an interesting challenge and a potentially rewarding drug discovery opportunity.[23] Using X-ray analysis of cocrystal structures, molecular modeling, site-directed mutagenesis, AChBP species differences, surface plasmon resonance (SPR) biosensor analysis, and isothermal titration calorimetry (ITC), we show that the thermodynamic signature of ligand binding changes drastically when the lobeline pocket is addressed. The obtained results illustrate that thermodynamic analysis of ligand binding provides important information about the binding mode and reveal the value of monitoring thermodynamic aspects during fragment growing.

RESULTS AND DISCUSSION

Chemistry. The designed compounds were prepared according to the route depicted in Scheme 1. Acylation of tropine with benzoyl chloride afforded tropine benzoate (**7**) in an excellent yield.[24] Subsequent demethylation using α-chloroethyl chloroformate gave the corresponding nortropinyl ester (**1**).[25] The α-hydroxylphenetyl extended fragment was synthesized by heating **1** with the (*R*)-enantiomer of phenyloxirane in the microwave.[26] The enantiomeric excess (ee) of **3** was determined at 98% by chiral HPLC. Reductive amination of phenylacetaldehyde with nortropine benzoate **1** using sodium triacetoxyborohydride as the reducing agent gave **4**.[27] Finally, treatment of **3** with iodomethane followed by recrystallization from chloroform resulted in isolation of the *endo*-α-(*R*)-hydroxyphenetyl-substituted quaternary ammonium derivative (**6**). The *endo*-configuration of the α-(*R*)-hydroxyphenetyl substituent was confirmed by 2D NMR.

Structure-Based Design of a Novel ligand that Interacts with the Lobeline Pocket. Fragment **1**, which is a structural analogue of hits that have been identified in an earlier study,[18] exhibits good LE (0.43 kcal·mol^{-1} per heavy atom) and was cocrystallized with Ac-AChBP. A 3.65 Å resolution crystal structure was obtained, with good density for the ligand (part a of Figure 2, and part a in both Figures S2 and S3 of the Supporting Information) despite the low resolution. The ability to use 5-fold restraints in crystallographic refinement allowed confident building of the compound into electron density, thus enabling structure-based optimization. The structure displays one Ac-AChBP pentamer per asymmetric unit where the C-loops adopt a closed conformation over all five binding sites. Fragment **1** is present at all five protomer−protomer interfaces, with similar orientations. The ligand is stabilized through hydrophobic interactions with Cys188, Cys189, Gln55, Ile116, and Tyr91, and through a hydrogen bond between the protonated amine atom of **1** and the backbone carbonyl from Trp145 (part a of Figures S1−S3 of the Supporting Information). When compared with lobeline-bound Ac-AChBP (part b of Figure 1, PDB: 2BYS), the fragment's benzoate group is tilted ∼50° with respect to lobeline's 1-phenylethanone moiety and stacked against the vicinal cysteines at the tip of loop C, placing the loop in a more open conformation (2.7 Å when comparing Cys188 Cα positions). The structure further reveals that gatekeeper residue Tyr91 is in the *g*-conformation, making the lobeline pocket inaccessible. From the complex structures, we predicted that further optimization of the fragment could be achieved by opening of and growing into the lobeline pocket (Figure 1). To address this subpocket, the fragment was merged with the α-hydroxyphenetyl group of lobeline (**2**),

dx.doi.org/10.1021/ja110571r |*J. Am. Chem. Soc.* 2011, 133, 5363–5371

Scheme 1

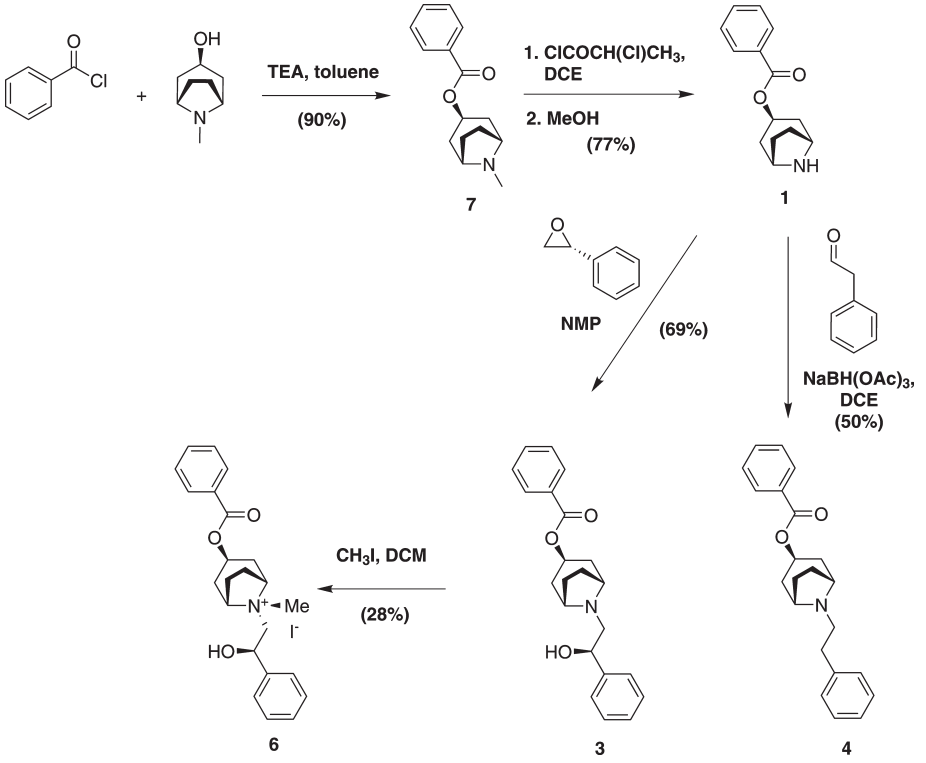

resulting in **3** (Figure 1). Molecular docking using *GOLD* (version 4.0)[28] suggests that the extended fragment **3** can adopt a binding mode in which the lobeline pocket is being addressed by the α-hydroxyphenetyl moiety (Figure S4 of the Supporting Information). Because these in silico results were promising, the designed compound was synthesized and screened for AChBP affinity.

X-ray Structures Confirm Insertion into the Lobeline Pocket. Extension of fragment **1** with an α-(*R*)-hydroxyphenetyl moiety yields **3** and resulted in a ∼50-fold increase in affinity ($pK_i = 7.0 \pm 0.1$), although the LE drops slightly from 0.43 to 0.37 kcal·mol^{-1} per heavy atom (part a of Figure 4). To confirm successful insertion into the lobeline pocket, a crystal structure of the optimized fragment (**3**) bound to Ac-AChBP was generated. The 3.59 Å resolution crystal structure shows that fragment **1** was successfully grown into the lobeline pocket (part b of Figure 2, and part b in both Figures S2 and S3 of the Supporting Information). The structure displays one pentamer in the asymmetric unit with each of the protomer−protomer interfaces binding one ligand molecule. The benzoate substituted nortropine moiety adopts an orientation similar to **1**, although displaced ∼1 Å deeper into the binding site, hence bringing loop C into a conformation intermediate between those observed for fragment **1** and lobeline Ac-AChBP complexes. Interestingly, an ion, most likely a chloride, could be refined in the position occupied by the lobeline 1-phenylethanone moiety from the lobeline−Ac-AChBP complex. Extension of fragment **1** with an α-(*R*)-hydroxyphenetyl moiety (resulting in **3**), induces a change in rotameric state of Tyr91 (*g*- to *t*-conformation) that opens the lobeline pocket. This tyrosine-flip is stabilized by hydrogen bond formation between the phenolic oxygen of Tyr91 and the side chain hydroxyl groups of Tyr53 and Ser165. The α-(*R*)-hydroxyphenetyl moiety responsible for the insertion into the lobeline pocket displays an orientation similar to that observed in the Ac-AChBP−lobeline complex and is involved in extensive hydrophobic interactions with Asp195, Tyr91, Lys141, Gly143, and Thr89 (part b of Figure 2, and part b in Figures S1−S3 of the Supporting Information). As a result, the experimentally determined binding mode corresponds very well to the predicted binding mode that was obtained by molecular docking (rmsd of 1.1 Å). Nevertheless, the experimentally determined binding mode differs from the predicted binding mode in that the hydroxyl group of **3** is not engaged in hydrogen bonding to the backbone carbonyl oxygens of Ser144 or Trp145 but instead is involved in van der Waals interactions with Tyr193 (Figure S4 of the Supporting Information).

Because the hydroxyl group of the optimized fragment **3** is not involved in formation of hydrogen bonds with the binding site, it was expected that its removal would lower the desolvation penalty and thereby result in an increase in binding affinity. The nor-hydroxyl derivative (**4**) was therefore synthesized and screened for AChBP affinity. Indeed, **4** exhibited higher AChBP affinity ($pK_i = 7.5 \pm 0$) than **3** and when compared with the starting fragment **1**, a 150-fold increase in binding affinity is observed (Figure 4). To determine if **4** induces the tyrosine-flip and interacts with the lobeline pocket, an additional cocrystal structure was generated. The **4**-Ac-AChBP structure was solved with a resolution of 3.30 Å and shows an almost identical binding mode to **3** (rmsd of 0.6 Å), exemplifying that a hydroxyl functionality is not required for opening of and insertion into the lobeline pocket (part c of Figure 2, and part c of both Figures S2 and S3 of the Supporting Information).

Site-Directed Mutagenesis Study on Stabilization of the Tyrosine-Flip. Visual inspection of the Ac-AChBP cocrystal structures of the optimized fragments **3** and **4** and the structure of the Ac-AChBP−lobeline complex by Hansen and co-workers[17] shows that the side chains of two residues (Tyr53 and Ser165) are likely to be involved in stabilization of the flipped state of

dx.doi.org/10.1021/ja110571r |*J. Am. Chem. Soc.* 2011, 133, 5363–5371

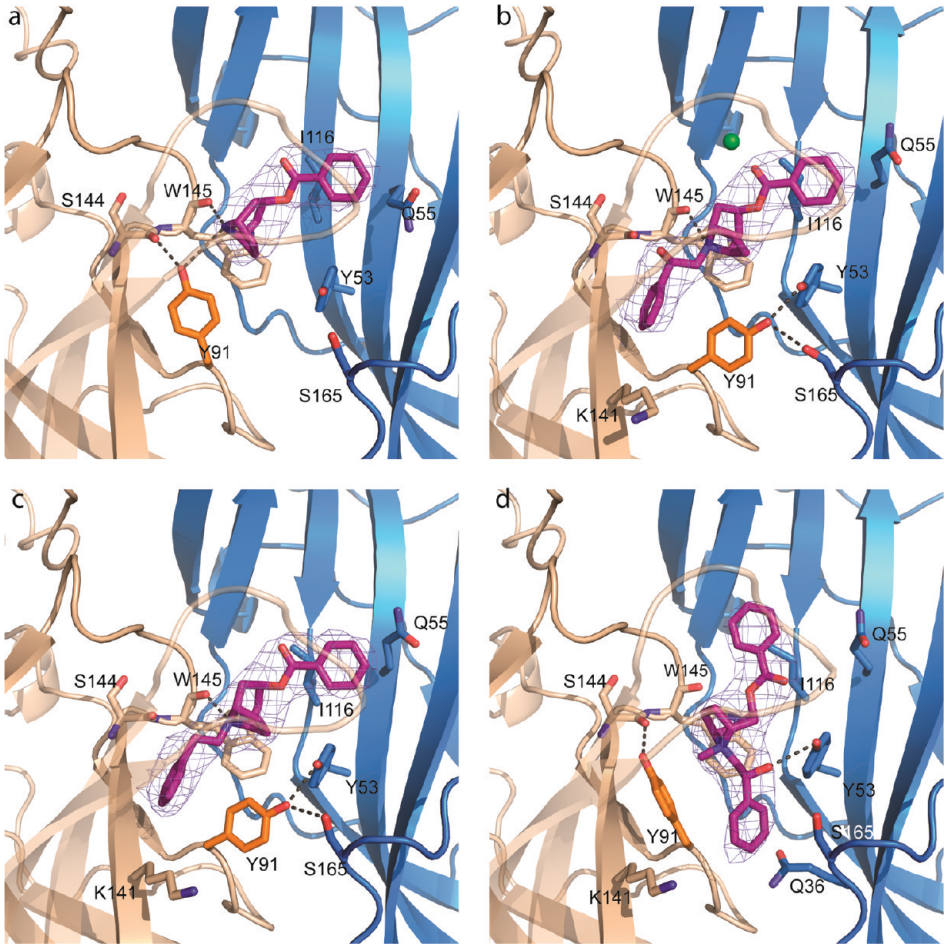

Figure 2. Growing fragment **1** into or away from the lobeline pocket. Cartoon representations of the Ac-AChBP complexes with fragment **1** (**a**), optimized fragments **3** (**b**) and **4** (**c**) and quaternary ammonium derivative **6** (**d**). The SigmaA weighted 2Fo−Fc electron density map at a 1σ level, carved 2 Å around the ligand is depicted as a mesh. The small sized fragment (**1**) does not interact with or induce an opening of the lobeline pocket and maintains the gatekeeper Tyr91 (orange sticks) into a *g*- state stabilized by a hydrogen bond with the Ser144 carbonyl (**a**). Growing into the lobeline pocket with **3** (**b**) or **4** (**c**) induces a change in rotameric state of Tyr91 (*g*- to *t* conformation), which opens the lobeline pocket. This tyrosine-flip is stabilized by hydrogen bond formation with the side chains of Tyr53 and Ser165 (**b**, **c**). The green sphere in (**b**) corresponds to a chloride ion. Quaternization of the tropine nitrogen of **3** with a methyl group, producing **6** locks the α-(*R*)-hydroxyphenetyl moiety in an *endo* configuration, unable to induce the opening of the lobeline pocket (**d**).

gatekeeper residue Tyr91 by hydrogen bond formation with the phenolic oxygen of Tyr91 (part b of Figure 1 and parts b and c of Figure 2). Superposition of X-ray structures of Ac-AChBP (PDB: 2BYS)[17] with its species variant Ls-AChBP (1UW6)[16] shows that the tyrosine-flip stabilizing residues, Tyr53 and Ser165, correspond to a tryptophan and a tyrosine (Trp53 and Tyr164) respectively in Ls-AChBP (Figure 3). The side chains of Trp53 and Tyr164 in Ls-AChBP are positioned in such a way that these residues are not able to stabilize the tyrosine-flip and hamper opening of the lobeline pocket in Ls-AChBP (Figure 3). To study the importance of Tyr53 and Ser165 in stabilizing the tyrosine-flip in Ac-AChBP, site-directed mutagenesis experiments were performed in which these residues were substituted for their Ls-AChBP counterparts, a tryptophan and a tyrosine, respectively. Affinity measurements of Ac-AChBP Y53W and S165Y mutants as well as wild-type Ac- and Ls-AChBPs were performed with nicotine and acetylcholine, which cannot interact with the lobeline pocket because of their small size, and with optimized fragment **3** and lobeline, which have been shown to interact with the lobeline pocket in Ac-AChBP from co-crystal structures. The results summarized in Table 1, indicate that Ser165 is essential for stabilizing the tyrosine-flip. Substitution of Tyr53 with a nonstabilizing tryptophan decreases the affinity of **3** by 5-fold and generates a small increase in affinity for the three other ligands. The switch from Ser165 to a nonstabilizing tyrosine has a more dramatic effect. The affinity for lobeline and compound **3** decreases by >400- and 25-fold respectively, whereas the affinities of acetylcholine and nicotine that do not interact with the lobeline pocket are hardly affected. Strikingly, this single point mutation in Ac-AChBP (S165Y) renders the affinity of **3** and lobeline very similar to wild type Ls-AChBP. These results provide strong evidence for a less accessible lobeline pocket in Ls-AChBP compared to Ac-AChBP.

Thermodynamic Analysis of Fragment Optimization Using SPR and ITC. The thermodynamic aspects of growing a fragment into the ligand-induced lobeline pocket of Ac-AChBP were studied by surface plasmon resonance (SPR) biosensor analyses, using an assay developed by Geitmann et al.,[29,30] at five different temperatures (15, 20, 25, 30, and 35 °C) and isothermal titration calorimetry (ITC). SPR at different temperatures allows dissection of binding affinity into the separate enthalpic and

dx.doi.org/10.1021/ja110571r |*J. Am. Chem. Soc.* 2011, 133, 5363–5371

entropic contributions using van't Hoff analysis[31−33] (van't Hoff plots are depicted in Figure S5 of the Supporting Information), whereas ITC analysis is directly related to enthalpic contribution and free energy and entropy are derived through titration curves[34] (Figure S6 of the Supporting Information). Our results on a large set of ligands show that these fundamentally different techniques result in very comparable profiles (Figure 4, Table 2). A major advantage of using SPR biosensor analysis is that this method requires substantially lower amounts of target protein compared to ITC.

Extending fragment **1** with an α-(*R*)-hydroxyl substituted phenetyl moiety (leading to **3**) results in a significant shift in thermodynamic binding signature where a large increase in favorable enthalpic contribution to the binding is observed for the optimized fragment **3** (part c of Figure 4 and Table 2). An even more enhanced increase in favorable enthalpic contribution is observed when extending the fragment with a phenetyl moiety (leading to **4**). These favorable enthalpic contributions are compensated to some extent by an unfavorable entropic contribution to the binding for both optimized ligands. A rationale for the difference in the enthalpic contributions to the binding between the two optimized ligands can be derived from crystal structures of the complexes of the two ligands to Ac-AChBP. These show that the hydroxyl group of **3** displays an unsatisfied hydrogen bond whereas the buried surface area is similar in both cases (~460 Å^2 calculated using the PISA webserver[35]), possibly causing the small difference in enthalpy.

Combining the thermodynamic analysis with the identified species differences, it was anticipated that complex formation to Ls-AChBP (nonstabilized tyrosine-flip) of lobeline, and optimized fragments **3** and **4** would be driven by less favorable enthalpy compared to Ac-AChBP (stabilized tyrosine-flip). Thermodynamic analysis using SPR biosensor analysis and ITC, confirmed our hypothesis. Binding of ligands that interact with the lobeline pocket in Ac-AChBP (**3**, **4** and lobeline) is characterized by more favorable enthalpy when compared to Ls-AChBP (parts c and d of Figure 4, Table 2). This is in contrast with ligands that do not interact with the lobeline pocket. Their binding to Ls-AChBP is driven by similar (nicotine) or more (fragment **1**) favorable enthalpy compared with binding to Ac-AChBP.

In addition, these results show that growing fragment **1** into the ligand-induced lobeline-pocket in Ac-AChBP renders the fragment selective for Ac-AChBP over Ls-AChBP. A plausible explanation for these observations that is in line with the site-directed mutagenesis results, is a differential stabilization of the *t*-conformation of gatekeeper residue between the AChBP species variants. As such, the lobeline pocket is better accessible in Ac-AChBP compared to Ls-AChBP and can be targeted as a species-selectivity subpocket.

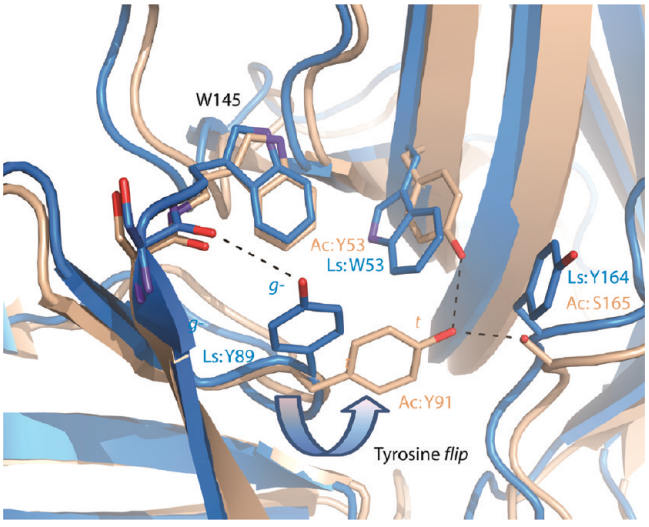

Figure 3. AChBP species differences in stabilization of the tyrosine-flip. The superposition of crystal structures of Ac-AChBP (in silicon) and Ls-AChBP (in blue) suggests that Trp53 and Tyr164 in Ls-AChBP (represented as blue sticks) cannot stabilize the tyrosine-flip contrary to Tyr53 and Ser165 in Ac-AChBP (represented as silicon sticks).

Ligand-Based Chemical Validation. Next to binding mode characterization by considering site-directed mutagenesis and species differences of the protein target, a ligand-based chemical validation of the conclusions was pursued. The X-ray cocrystal structure of the optimized fragment **3** shows that in order to interact with the lobeline pocket the α-(*R*)-hydroxyphenetyl moiety takes an *exo*-configuration with respect to the tropine moiety, that is the substituent that is inserted into the lobeline pocket is pointing toward the tropine ethylene bridge (part b of Figure 2). Quaternization of the tropine nitrogen atom of **3** by introduction of an additional methyl substituent, prevents pyramidal inversion and locks the α-(*R*)-hydroxyphenetyl moiety in the opposite *endo*-configuration, which is anticipated to prevent this derivative from interacting with the lobeline pocket (chemical synthesis and characterization is described in the Supporting Information). Interestingly, pharmacological screening using [^{3}H]-epibatine displacement shows that upon quaternization of the basic amine of **3** affording compound **6**, the affinity for Ac-AChBP is lowered 10-fold, whereas affinity for Ls-AChBP increases 6-fold (part a of Figure 4). This minor modification, that is addition of a single methyl substituent renders **3** from 8-fold *Aplysia*-selective to 8-fold selective for the *Lymnaea*-AChBP species. The cocrystal structure of the quaternary methylammonium derivative **6** with Ac-AChBP was solved to a resolution of 3.25 Å and provides an explanation for the observed change in AChBP species selectivity. Quaternary ammonium

Table 1. Investigation of AChBP Species Differences Using Site-Directed Mutagenesis

	pK_i ± SEM[a]			
	Ac-wt	Ac-Y53W	Ac-S165Y	Ls-wt
α-lobeline (**2**)	8.5 ± 0.1	8.7 ± 0.1	5.9 ± 0.1	6.2 ± 0.1
3	7.0 ± 0.1	6.3 ± 0.1	5.6 ± 0.1	6.2 ± 0.1
acetylcholine	4.0 ± 0.1	4.5 ± 0.1	4.3 ± 0.1	5.2 ± 0.1
nicotine (**5**)	5.6 ± 0.1	6.3 ± 0.1	5.5 ± 0.1	6.4 ± 0.1

[a] pK_i values ±SEM over 3 radioligand displacement experiments using [^{3}H]-epibatidine.

dx.doi.org/10.1021/ja110571r |*J. Am. Chem. Soc.* 2011, 133, 5363–5371

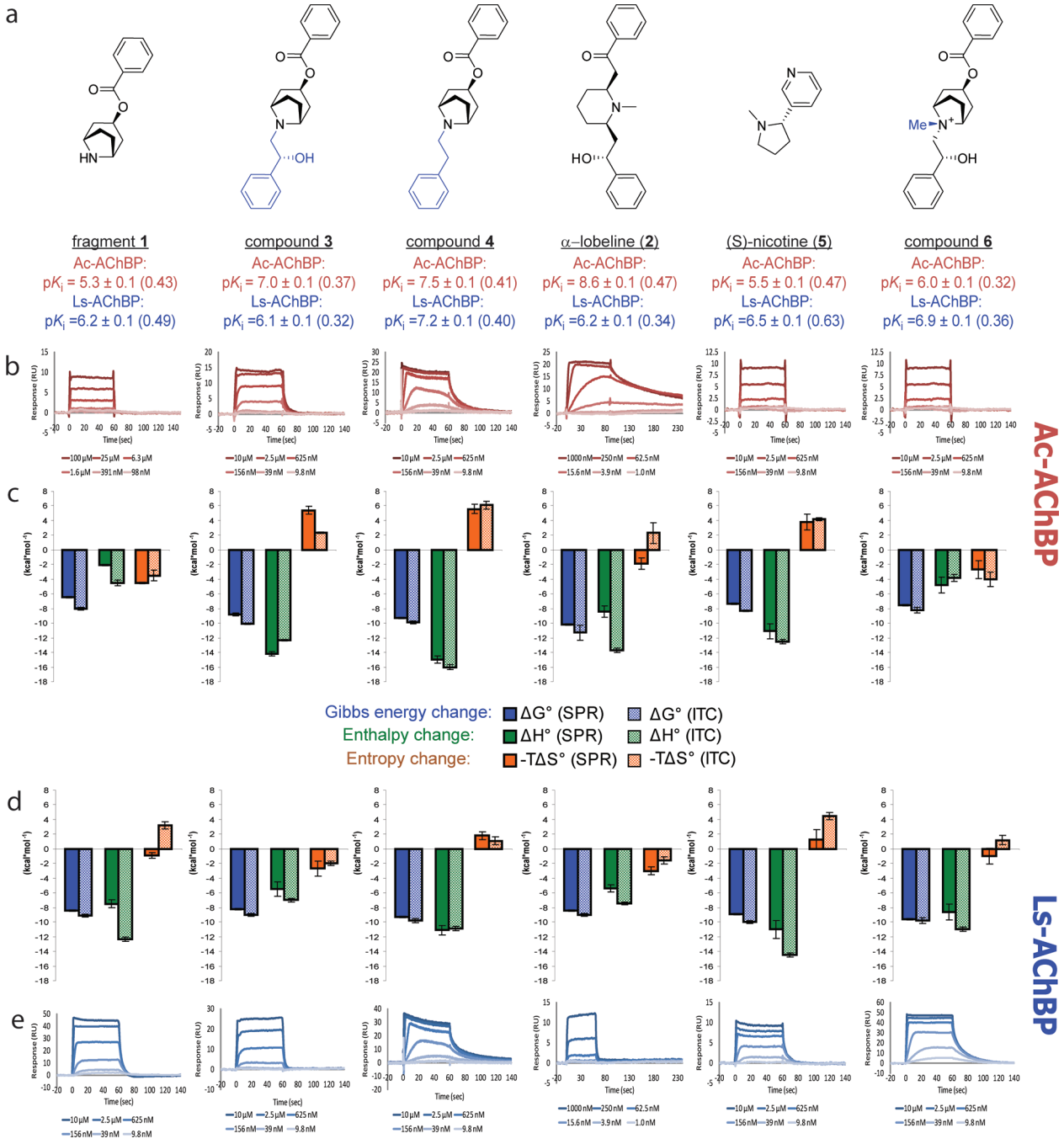

Figure 4. (**a**) Chemical structures and binding affinities for Ac-AChBP and Ls-AChBP as determined by [^{3}H]-epibatidine displacement of the compounds that were evaluated using SPR biosensor analysis and ITC. Ligand efficiency (LE) of each compound is depicted between brackets in kcal·mol^{-1} per heavy atom. (**b**) Representative sensorgrams of the compounds binding to Ac-AChBP at different concentrations at 25 °C. Thermodynamic profiles for ligand binding to Ac-AChBP (**c**) and Ls-AChBP (**d**) were obtained using SPR biosensor analysis (dark bars ± SEM) and ITC (light bars ± fitting errors) and are represented in bar charts. Shown are the changes that occur upon ligand binding in Gibbs energy ($\Delta G°$) (SPR, dark blue; ITC, light blue), enthalpy ($\Delta H°$) (SPR, dark green; ITC, light green) and entropic contributions ($-T\Delta S°$) (SPR, dark red; ITC, light red). All thermodynamic parameters shown are in kcal·mol^{-1}. (**e**) Representative sensorgrams of the four compounds binding to Ls-AChBP at different concentrations at 25 °C.

derivative **6** was present in the five protomer−protomer interfaces with similar orientations, showing that the quaternized ligand does not interact with the lobeline pocket. In this complex, Tyr91 adopts a *g*- conformation with a χ_2 value of −30°, and is stabilized through a hydrogen bond between the phenolic hydroxyl group and the carbonyl group from the Ser144 backbone (part d of Figure 2, part d of both Figures S2 and S3 of the Supporting Information). Such an orientation of the Tyr91 side chain is indicative of an inaccessible lobeline pocket. Furthermore, in this complex Tyr91 adopts a different rotamer state from the one observed in the Ac-AChBP- complex with fragment **1** ($\chi_2 = -85°$) likely to accommodate the methyl group

dx.doi.org/10.1021/ja110571r |*J. Am. Chem. Soc.* 2011, 133, 5363–5371

Table 2. Thermodynamic Parameters of Binding at 25 °C[a]

	compound	method	pK_D	$\Delta G°$(kcal·mol^{-1})	$\Delta H°$ (kcal·mol^{-1})	$-T\Delta S°$ (kcal·mol^{-1})
Ac-AChBP	1	SPR	4.7 ± 0.1	−6.5 ± 0.1	−2.1 ± 0.1	−4.5 ± 0.1
		ITC	5.9 ± 0.2	−8.0 ± 0.2	−4.5 ± 0.4	−3.5 ± 0.7
	3	SPR	6.5 ± 0.1	−8.8 ± 0.2	−14.2 ± 0.3	5.4 ± 0.5
		ITC	7.4 ± 0.1	−10.1 ± 0.1	−12.3 ± 0.1	2.3 ± 0.1
	4	SPR	6.9 ± 0.1	−9.3 ± 0.1	−15.0 ± 0.5	5.6 ± 0.6
		ITC	7.3 ± 0.2	−9.9 ± 0.2	−16.0 ± 0.3	6.1 ± 0.5
	α-lobeline (2)	SPR	7.5 ± 0.1	−10.2 ± 0.1	−8.4 ± 0.8	−1.9 ± 0.8
		ITC	8.3 ± 0.3	−11.3 ± 1.0	−13.7 ± 0.3	2.3 ± 1.4
	(*S*)-nicotine (5)	SPR	5.3 ± 0.1	−7.3 ± 0.1	−11.1 ± 1.0	3.8 ± 1.1
		ITC	6.1 ± 0.1	−8.3 ± 0.1	−12.5 ± 0.3	4.2 ± 0.2
	6	SPR	5.5 ± 0.1	−7.5 ± 0.1	−4.8 ± 1.1	−2.7 ± 1.2
		ITC	6.0 ± 0.4	−8.2 ± 0.4	−3.8 ± 0.5	−4 ± 1
Ls-AChBP	1	SPR	6.1 ± 0.1	−8.4 ± 0.1	−7.5 ± 0.5	−0.9 ± 0.4
		ITC	6.7 ± 0.2	−9.1 ± 0.2	−12.3 ± 0.3	3.2 ± 0.5
	3	SPR	6.0 ± 0.1	−8.2 ± 0.1	−5.5 ± 1.0	−2.7 ± 1.0
		ITC	6.6 ± 0.2	−9.0 ± 0.2	−7.0 ± 0.2	−2.0 ± 0.3
	4	SPR	6.8 ± 0.1	−9.3 ± 0.1	−11.1 ± 0.6	1.8 ± 0.5
		ITC	7.2 ± 0.2	−9.8 ± 0.3	−10.9 ± 0.3	1.1 ± 0.5
	α-lobeline (2)	SPR	6.1 ± 0.1	−8.4 ± 0.1	−5.4 ± 0.5	−3.0 ± 0.5
		ITC	6.6 ± 0.1	−9.0 ± 0.2	−7.4 ± 0.2	−1.6 ± 0.5
	(*S*)-nicotine (5)	SPR	6.5 ± 0.1	−8.9 ± 0.1	−11.0 ± 1.2	1.3 ± 1.3
		ITC	7.3 ± 0.2	−10.0 ± 0.2	−14.5 ± 0.3	4.5 ± 0.5
	6	SPR	7.0 ± 0.1	−9.6 ± 0.1	−8.6 ± 1.1	−1.0 ± 1.1
		ITC	7.2 ± 0.3	−9.8 ± 0.4	−11.0 ± 0.3	1.2 ± 0.6

[a] SPR values are ± SEM over multiple experiments (n = 3−6). ITC values are ± fitting errors.

tethered to the amine of VUF11438. The quaternized nitrogen of ligand **6** can make cation−π interactions with Trp145, Tyr91, Tyr186, Tyr193, and Tyr53, whereas a hydrogen bond is made between the hydroxyl group of the ligand and of Tyr53. The benzoate moiety of **6** is oriented differently in the binding site in an intermediate position relative to the benzoate of optimized fragments **3** or **4** and the lobeline 1-phenylethanone moiety, where it interacts via hydrophobic contacts with Ile116, Met114, and the vicinal Cys188 and Cys 189 at the tip of loop C.

In line with these findings, is the thermodynamic data that reveals that the favorable enthalpy of binding of compound **3** to Ac-AChBP is dramatically reduced upon quaternization, leading to ligand **6**. However, the entropy of binding becomes more favorable limiting the loss in affinity upon quaternization of **3** to 10-fold when binding to Ac-AChBP (parts a and c of Figure 4). In the case of Ls-AChBP and in contrast with Ac-AChBP, quaternization of compound **3** affords a favorable change in enthalpy. As a result, the quaternary ammonium derivative **6** binds with more favorable enthalpy to Ls-AChBP compared to Ac-AChBP. Similar to what is observed with ligands not interacting with the lobeline pocket such as fragment **1**, but not with ligands addressing the lobeline pocket such as lobeline **2**, **3**, and **4**. The more favorable enthalpic contribution possibly arises from the differences in the complementary binding sites of Ls- and Ac-AChBP, such as the replacement of Tyr53 by a tryptophan or of Ile116 by a methionine. Such variations are likely to significantly alter the interaction interface with the binding site and may be of influence to the binding mode.

Integrating the X-ray data on the Ac-AChBP cocrystal complexes of the optimized fragments **3** and **4** with the thermodynamic analysis and site-directed mutagenesis results, provides evidence that the change in thermodynamic binding signature upon fragment optimization is indicative of interactions with the ligand-induced AChBP subpocket. Ligand **4** binds with similar affinity to Ac-AChBP and Ls-AChBP. The affinity data therefore does not provide any indication for a difference in binding modes. However, the changes in binding enthalpy upon extending fragment **1** with a phenetyl moiety (resulting in **4**) are substantially different for Ac-AChBP ($\Delta\Delta H°$ = −12.9 kcal·mol^{-1} (SPR), −11.5 kcal·mol^{-1} (ITC)) compared to Ls-AChBP ($\Delta\Delta H°$ −3.6 kcal·mol^{-1} (SPR), +1.4 kcal·mol^{-1} (ITC)). The significant favorable change in enthalpy for Ac-AChBP, upon extending fragment VUF10663 with a phenetyl moiety is likely to result from interactions with the ligand-induced AChBP subpocket. The site-directed mutagenesis results strongly indicate that the lobeline pocket is less accessible in Ls-AChBP compared to Ac-AChBP. Therefore, we propose, that because of a distinct binding mode in Ls-AChBP, in which the lobeline pocket is not addressed, no significant favorable change in enthalpy, upon extension of fragment **1** by a phenetyl moiety is observed. In line with this proposal are the thermodynamic changes upon growing fragment **1** into the quaternary ammonium derivative **4**. This chemical modification prevents the ligand from interacting with the lobeline pocket in Ac-AChBP, and yields similar changes in enthalpy for Ac-AChBP ($\Delta\Delta H°$ −2.7 kcal·mol^{-1} (SPR), −1.1 kcal·mol^{-1} (ITC)) and Ls-AChBP ($\Delta\Delta H°$ −1.1 kcal·mol^{-1} (SPR), +1.3 kcal·mol^{-1} (ITC)) (Figure 5). As such, these results illustrate that more than affinity data alone, thermodynamic analysis and focus on enthalpic and entropic contributions during fragment optimization can provide valuable information on the

dx.doi.org/10.1021/ja110571r |*J. Am. Chem. Soc.* 2011, 133, 5363–5371

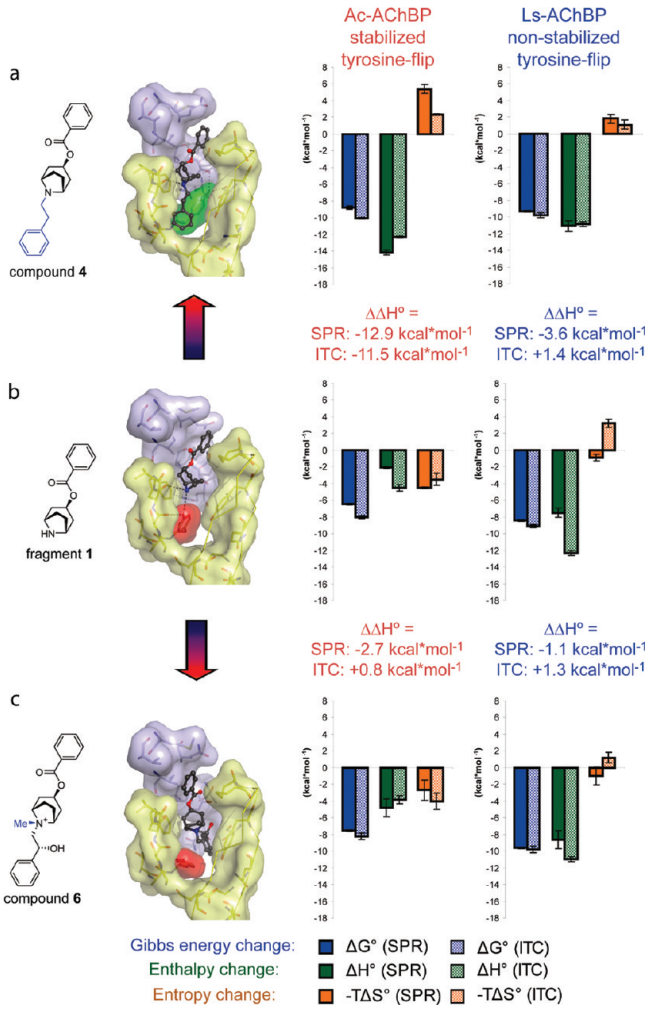

Figure 5. Thermodynamic analysis provides indication of successful insertion into the lobeline pocket. Chemical structures and binding modes as determined by X-ray analysis of Ac-AChBP cocrystal structures and the thermodynamic binding signatures for Ac-AChBP and Ls-AChBP of optimized fragment **4** (**a**) fragment **1** (**b**) and quaternary ammonium derivative **6** (**c**) as determined by SPR biosensor analysis (dark bars ± SEM) and ITC (light bars ± fitting errors). Shown are the changes that occur upon ligand binding in Gibbs energy ($\Delta G°$) (SPR, dark blue; ITC, light blue), enthalpy ($\Delta H°$) (SPR, dark green; ITC, light green) and entropic contributions ($-T\Delta S°$) (SPR, dark red; ITC, light red). All thermodynamic parameters shown are in kcal·mol^{-1}.

binding mode of a ligand, thereby better guiding the rational design process.

In the current study, we have grown a hit fragment into a protein binding pocket that can be induced by triggering conformational changes of the protein. X-ray analysis confirmed the successful design strategy. Thermodynamic binding analysis showed that insertion into the lobeline pocket by extending fragment **1** with a hydrophobic phenetyl moiety resulting in **4** affords a considerable favorable change in enthalpy of ∼−12 kcal·mol^{-1}, that is partly compensated by an entropic penalty. This is in contrast with the classical view on the hydrophobic effect, in which increased burial of hydrophobic moieties in a hydrophobic pocket results in favorable changes in entropy. Studies on major mouse urinary protein suggest that enthalpy driven hydrophobic association results from poor solvation of the binding site, prior to complex formation.[36−38] The apo-Ac-AChBP X-ray structure (pdb: 2W8E)[18] shows that residue Tyr91 is in the *g*-conformation and functions as a gatekeeper making the lobeline pocket inaccessible. It is therefore likely that, before complex formation, the lobeline pocket is poorly solvated. A significant part of the extensive favorable change in enthalpy may therefore result from strong van der Waals interactions between the phenetyl moiety of **4** and the lobeline pocket that are not compensated by the solvent.

Besides providing insight into the thermodynamic aspects of fragment growing, our investigations also reveal that growing the fragment **1** into the lobeline pocket renders the fragment selective for Ac-AChBP, whereas introduction of an additional methyl substituent preventing interactions with the lobeline pocket reverses the AChBP species selectivity back to *Lymnaea*. Thus, selectivity for Ac-AChBP over Ls-AChBP can be achieved by addressing the lobeline pocket. The subtle differences in protein conformational changes that induce the lobeline pocket may be of interest in the design of subtype-selective ligands for human nicotinic receptors as well. The gatekeeper tyrosine residue is conserved among the human nAChR subtypes, whereas the residue (Ser165 in Ac-AChBP) that stabilizes the open lobeline pocket conformation is located in a highly variable region. As can be seen from part a of Figure 4, lobeline exerts a 250-fold selectivity for Ac-AChBP (accessible lobeline pocket) over Ls-AChBP (inaccessible lobeline pocket) and ∼1000-fold selectivity for $\alpha4\beta2$ over $\alpha7$ nAChRs.[39,40] Differential stabilization of the rotameric states of the gatekeeper tyrosine residue may provide an explanation for the observed nAChR subtype selectivity of lobeline and the lobeline pocket may be targeted as a subtype-selectivity pocket.

CONCLUSIONS

The work described here illustrates that fragment growing can trigger ligand-induced conformational changes of the target protein. The obtained results strongly indicate that the distinct changes in thermodynamic binding signatures upon fragment optimization between Ac-AChBP and Ls-AChBP result from a difference in binding modes of the optimized fragments. We conclude that, more than affinity data alone, dissection of binding affinity into the separate enthalpic and entropic contributions provides valuable information with regard to the binding mode of a ligand. Furthermore, our studies show that thermodynamic analysis, enabled by state-of-the-art technologies such as ITC and SPR biosensor analysis, in our hands give comparable results. Altogether, this study illustrates that, in combination with detailed structural information (X-ray of cocrystals), thermodynamic data provides crucial insights that enable efficient fragment optimization.

ASSOCIATED CONTENT

Supporting Information. Complete refs 10 and 11, full experimental details, crystallographic data and refinement statistics, van't Hoff plots, and ITC titration curves. This material is available free of charge via the Internet at http://pubs.acs.org. The new AChBP cocrystal structures described in this paper have been deposited in the Protein Data Bank (PDB codes 2Y54, 2Y56, 2Y57, and 2Y58).

AUTHOR INFORMATION

Corresponding Author
i.de.esch@few.vu.nl

Author Contributions

[#]These authors contributed equally.

■ ACKNOWLEDGMENT

This work was supported by a grant of the Top Institute Pharma D2-103 (to A.B.S.), and received funding from the European Union Seventh Framework Programme under grant agreement no. HEALTH-F2-2007-202088 ("NeuroCypres" project). P.R. was supported by a long term fellowship from the European Molecular Biology Organization. We thank Eric Karssen for chemical synthesis of compound **3**, Frans J.J. de Kanter for performing 2D NMR measurements, and Chris Oostenbrink and Chimed Janssen for useful discussions on thermodynamic aspects of ligand−protein interactions. We thank staff from SLS PX1 and ESRF ID23-2 for their assistance during data collection, Robbie Joosten for useful discussion during structure validation steps, and Patrick Celie for help with ITC measurements.

■ REFERENCES

(1) de Kloe, G. E.; Bailey, D.; Leurs, R.; de Esch, I. J. *Drug Discov. Today* **2009**, *14*, 630–46.
(2) Erlanson, D. A. *Curr. Opin. Biotechnol.* **2006**, *17*, 643–52.
(3) Hajduk, P. J.; Greer, J. *Nat. Rev. Drug Discov.* **2007**, *6*, 211–9.
(4) Congreve, M.; Carr, R.; Murray, C.; Jhoti, H. *Drug Discov. Today* **2003**, *8*, 876–7.
(5) Schuffenhauer, A.; Ruedisser, S.; Marzinzik, A. L.; Jahnke, W.; Blommers, M.; Selzer, P.; Jacoby, E. *Curr. Top. Med. Chem.* **2005**, *5*, 751–62.
(6) Chung, S.; Parker, J. B.; Bianchet, M.; Amzel, L. M.; Stivers, J. T. *Nat. Chem. Biol.* **2009**, *5*, 407–13.
(7) Howard, N.; Abell, C.; Blakemore, W.; Chessari, G.; Congreve, M.; Howard, S.; Jhoti, H.; Murray, C. W.; Seavers, L. C.; van Montfort, R. L. *J. Med. Chem.* **2006**, *49*, 1346–55.
(8) Congreve, M.; Chessari, G.; Tisi, D.; Woodhead, A. J. *J. Med. Chem.* **2008**, *51*, 3661–80.
(9) Sledz, P.; Silvestre, H. L.; Hung, A. W.; Ciulli, A.; Blundell, T. L.; Abell, C. *J. Am. Chem. Soc.* **2010**, *132*, 4544–5.
(10) Wang, Y. S.; et al. *J. Med. Chem.* **2010**, *53*, 942–50.
(11) Zhu, Z.; et al. *J. Med. Chem.* **2010**, *53*, 951–65.
(12) Rucktooa, P.; Smit, A. B.; Sixma, T. K. *Biochem. Pharmacol.* **2009**, *78*, 777–87.
(13) Sixma, T. K.; Smit, A. B. *Annu. Rev. Biophys. Biomol. Struct.* **2003**, *32*, 311–34.
(14) Brejc, K.; van Dijk, W. J.; Klaassen, R. V.; Schuurmans, M.; van Der Oost, J.; Smit, A. B.; Sixma, T. K. *Nature* **2001**, *411*, 269–76.
(15) Celie, P. H.; Kasheverov, I. E.; Mordvintsev, D. Y.; Hogg, R. C.; van Nierop, P.; van Elk, R.; van Rossum-Fikkert, S. E.; Zhmak, M. N.; Bertrand, D.; Tsetlin, V.; Sixma, T. K.; Smit, A. B. *Nat. Struct. Mol. Biol.* **2005**, *12*, 582–8.
(16) Celie, P. H.; van Rossum-Fikkert, S. E.; van Dijk, W. J.; Brejc, K.; Smit, A. B.; Sixma, T. K. *Neuron* **2004**, *41*, 907–14.
(17) Hansen, S. B.; Sulzenbacher, G.; Huxford, T.; Marchot, P.; Taylor, P.; Bourne, Y. *EMBO J.* **2005**, *24*, 3635–46.
(18) Ulens, C.; Akdemir, A.; Jongejan, A.; van Elk, R.; Bertrand, S.; Perrakis, A.; Leurs, R.; Smit, A. B.; Sixma, T. K.; Bertrand, D.; de Esch, I. J. *J. Med. Chem.* **2009**, *52*, 2372–83.
(19) Celie, P. H.; Klaassen, R. V.; van Rossum-Fikkert, S. E.; van Elk, R.; van Nierop, P.; Smit, A. B.; Sixma, T. K. *J. Biol. Chem.* **2005**, *280*, 26457–66.
(20) Hopkins, A. L.; Groom, C. R.; Alex, A. *Drug Discov. Today* **2004**, *9*, 430–1.
(21) Dutertre, S.; Ulens, C.; Buttner, R.; Fish, A.; van Elk, R.; Kendel, Y.; Hopping, G.; Alewood, P. F.; Schroeder, C.; Nicke, A.; Smit, A. B.; Sixma, T. K.; Lewis, R. J. *EMBO J.* **2007**, *26*, 3858–67.
(22) Lovell, S. C.; Word, J. M.; Richardson, J. S.; Richardson, D. C. *Proteins* **2000**, *40*, 389–408.
(23) Kallblad, P.; Dean, P. M. *J. Mol. Biol.* **2003**, *326*, 1651–65.
(24) Maksay, G.; Nemes, P.; Biro, T. *J. Med. Chem.* **2004**, *47*, 6384–91.
(25) Howarth, N. M.; Malpass, J. R.; Smith, C. R. *Tetrahedron* **1998**, *54*, 10899–10914.
(26) Couturier, M.; Tucker, J. L. *Tetrahedron: Asymmetry* **2003**, *14*, 3517–3523.
(27) Abdel-Magid, A. F.; Carson, K. G.; Harris, B. D.; Maryanoff, C. A.; Shah, R. D. *J. Org. Chem.* **1996**, *61*, 3849–3862.
(28) Verdonk, M. L.; Cole, J. C.; Hartshorn, M. J.; Murray, C. W.; Taylor, R. D. *Proteins* **2003**, *52*, 609–23.
(29) Geitmann, M.; Retra, K.; de Kloe, G. E.; Homan, E.; Smit, A. B.; de Esch, I. J.; Danielson, U. H. *Biochemistry* **2010**, *49*, 8143–54.
(30) Retra, K.; Geitmann, M.; Kool, J.; Smit, A. B.; de Esch, I. J.; Danielson, U. H.; Irth, H. *Anal. Biochem.* **2010**, *407*, 58–64.
(31) Roos, H.; Karlsson, R.; Nilshans, H.; Persson, A. *J. Mol. Recognit.* **1998**, *11*, 204–10.
(32) Shuman, C. F.; Hamalainen, M. D.; Danielson, U. H. *J. Mol. Recognit.* **2004**, *17*, 106–19.
(33) Zhukov, A.; Karlsson, R. *J. Mol. Recognit.* **2007**, *20*, 379–85.
(34) O'Brien, R.; Ladbury, J. E.; B.Z., C. *Protein−Ligand Interactions*; Oxford University Press: New York, 2000; 263−284.
(35) Krissinel, E.; Henrick, K. *J. Mol. Biol.* **2007**, *372*, 774–97.
(36) Barratt, E.; Bingham, R. J.; Warner, D. J.; Laughton, C. A.; Phillips, S. E.; Homans, S. W. *J. Am. Chem. Soc.* **2005**, *127*, 11827–34.
(37) Bingham, R. J.; Findlay, J. B.; Hsieh, S. Y.; Kalverda, A. P.; Kjellberg, A.; Perazzolo, C.; Phillips, S. E.; Seshadri, K.; Trinh, C. H.; Turnbull, W. B.; Bodenhausen, G.; Homans, S. W. *J. Am. Chem. Soc.* **2004**, *126*, 1675–81.
(38) Sharrow, S. D.; Novotny, M. V.; Stone, M. J. *Biochemistry* **2003**, *42*, 6302–9.
(39) Miller, D. K.; Crooks, P. A.; Zheng, G.; Grinevich, V. P.; Norrholm, S. D.; Dwoskin, L. P. *J. Pharmacol. Exp. Ther.* **2004**, *310*, 1035–45.
(40) Zheng, G.; Dwoskin, L. P.; Deaciuc, A. G.; Norrholm, S. D.; Crooks, P. A. *J. Med. Chem.* **2005**, *48*, 5551–60.